Original Article

First-in-human results of targeted intraoperative molecular imaging for visualization of ground glass opacities during robotic pulmonary resection

Gregory T. Kennedy[1], Feredun S. Azari[1], Elizabeth Bernstein[1], Isvita Marfatia[1], Azra Din[1], Charuhas Deshpande[2], Nikki Galvis[3], Jonathan Sorger[3], John C. Kucharczuk[1], Sunil Singhal[1]

[1]Department of Surgery, University of Pennsylvania Perelman School of Medicine, Philadelphia, PA, USA; [2]Department of Pathology, University of Pennsylvania Perelman School of Medicine, Philadelphia, PA, USA; [3]Intuitive Surgical, Sunnyvale, CA, USA

Contributions: (I) Conception and design: GT Kennedy, S Singhal; (II) Administrative support: E Bernstein, I Marfatia, A Din; (III) Provision of study materials or patients: GT Kennedy, C Deshpande, N Galvis, J Sorger, JC Kucharczuk, S Singhal; (IV) Collection and assembly of data: GT Kennedy, FS Azari, E Bernstein, I Marfatia, A Din, C Deshpande, S Singhal; (V) Data analysis and interpretation: GT Kennedy, FS Azari, E Bernstein, S Singhal; (VI) Manuscript writing: All authors; (VII) Final approval of manuscript: All authors.

Correspondence to: Sunil Singhal, MD. Department of Surgery, Perelman School of Medicine, 3400 Spruce Street, 6 White Building, Philadelphia, PA 19104, USA. Email: Sunil.Singhal@pennmedicine.upenn.edu.

Background: Identifying ground glass opacities (GGOs) is challenging during robot-assisted thoracic surgery (RATS). Intraoperative molecular imaging (IMI) using tumor-targeted fluorescent tracers may address this clinical problem, but has never been evaluated in RATS. In a pilot study, we sought to determine whether IMI during RATS (RIMI) can localize GGOs.

Methods: Ten patients with a cT1 GGO were enrolled. Prior to resection, participants received a folate-receptor targeted fluorescent tracer (OTL38). During RATS, a white-light robotic scope was utilized to identify tumors. RIMI was then conducted using a RATS thoracoscope with a wavelength-specific camera. Finally, a video-assisted thoracic surgery (VATS) thoracoscope designed to detect OTL38 was used as a control to compare to RIMI. The lesions were then resected under RIMI guidance.

Results: By white-light robotic scope, 7/10 (70%) GGOs were visually identifiable by pleuroparenchymal distortions. RIMI identified tumor-specific fluorescence in all (100%) subjects. RIMI clearly located the three nodules that could not be seen by robotic white-light imaging. The mean fluorescence intensity (MFI) of tumors was 99.48 arbitrary units (A.U.) (IQR, 75.72–130.49 A.U.), which was significantly higher than background tissue with mean MFI 20.61 A.U. (IQR, 13.49–29.93 A.U., P<0.0001). Mean signal-to-background ratio was 5.71 (range, 2.28–10.13). When compared to VATS-IMI as a control, there were no significant differences in MFI of tumors, background tissue, or signal-to-background ratios. In summary, RIMI compared favorably to VATS-IMI by all measured imaging characteristics.

Conclusions: RIMI is feasible for identification of GGOs during robotic resection as compared to white light thoracoscopy and compares favorably to VATS-IMI.

Keywords: Intraoperative molecular imaging (IMI); robotic surgery; lung cancer

Submitted Dec 17, 2021. Accepted for publication Mar 20, 2022.
doi: 10.21037/tlcr-21-1004
View this article at: https://dx.doi.org/10.21037/tlcr-21-1004

Introduction

With expanded guidelines for computed tomography screening for lung cancer, a vast number of suspicious ground glass opacity pulmonary nodules are detected annually (1,2). These lesions often require resection for diagnosis, which can be curative in early stage disease (3). Intraoperative localization of lesions is of paramount importance, given growing evidence that sublobar resection with appropriate margins has equivalent survival benefit to formal lobectomy (4-6). However, accurate intraoperative localization can be difficult in cases of early stage lesions and ground glass opacities that are only marked by subtle parenchymal distortions (3,7). These challenges are further exacerbated in robotic surgery due to its lack of haptic feedback from finger palpation (8,9).

Previous attempts to improve localization of non-palpable tumors—including endoscopic or transthoracic placement of hook wires, fiducials, or fluoroscopic dyes—have shown limited efficacy with a well-documented side effect profile including bleeding, device dislodgement, and additional radiation exposure (10).

Our group has been exploring intraoperative molecular imaging during video-assisted thoracic surgery (VATS-IMI) as an alternative technology to highlight tumors during surgery (11-16). VATS-IMI uses targeted fluorescent tracers that selectively accumulate in malignant cells and can be visualized using a wavelength-specific thoracoscope during surgery (17,18). One of the most promising agents is a near-infrared folate receptor (FR) targeted tracer, OTL38 (19). This tracer is designed to improve visualization of pulmonary adenocarcinomas, which express FRα at 105 fold higher than surrounding lung parenchyma (20). We have also found it to be effective in highlighting pulmonary squamous cell carcinomas, small cell lung cancer, and granulomas via labeling of tumor-associated macrophages which express folate receptor beta (21,22). A Phase 1 trial of IMI using OTL38 in 20 patients demonstrated that IMI is safe and feasible in patients undergoing resection of pulmonary adenocarcinomas (23). A subsequent multi-institutional Phase 2 trial of 110 patients showed that IMI was effective in improving operative outcomes for patients by detecting synchronous lesions not identified on preoperative imaging, localizing non-palpable, visually occult lesions, or identifying tumor-positive margins (24).

Here, we report the first use of IMI to localize ground glass opacities (GGOs) during robotic assisted thoracic surgery (RATS). We conducted a pilot study in 10 patients undergoing resection of small GGOs. We hypothesized that IMI during robotic-assisted thoracic surgery (RIMI) could provide accurate nodule localization in patients with small ground glass opacities, and thereby facilitate sublobar resection in the absence of tactile feedback. We compared the performance of RIMI to the VATS-IMI technique, as a control. This was not a comparison of RATS to VATS, as this has been extensively studied in the literature, but rather a means to compare the novel technique of RIMI to a validated IMI technology. We present the following article in accordance with the TREND reporting checklist (available at https://tlcr.amegroups.com/article/view/10.21037/tlcr-21-1004/rc).

Methods

Summary of study design

Figure 1 provides an overview of the study design. Study design and study size were based on consensus guidelines provided by the World Molecular Imaging Society (25). The primary objective was the ability of RIMI to localize GGOs during robotic surgery and secondary aims included comparison of fluorescence imaging quality to existing VATS IMI technology. The study was conducted in accordance with the Declaration of Helsinki (as revised in 2013). The study was approved by the University of Pennsylvania Institutional Review Board (IRB Approval Number: 822153) and all patients gave written informed consent. Ten patients with a T1 (<3 cm) pulmonary lesion suspicious for malignancy and with radiographic features suggestive of a ground glass opacity with or without solid component were enrolled between November 2020 and February 2021. Exclusion criteria included people under the age of 18, people unable to give informed consent, non-English-speaking people, and patients with prior chest surgery. Patients presenting with multifocal GGOs were also excluded from the study.

All identified subjects underwent preoperative high-resolution CT scanning which was reviewed by a thoracic radiologist to confirm the presence of a pulmonary nodule and identify other suspicious nodules. Each subject also underwent preoperative 18FDG-positron emission tomography (PET). For imaging studies obtained outside the University of Pennsylvania Health System (UPHS), at least one UPHS thoracic radiologist reviewed preoperative imaging to confirm the presence of pulmonary nodules, rule-out synchronous disease, and confirm findings of 18FDG-positron emission tomography.

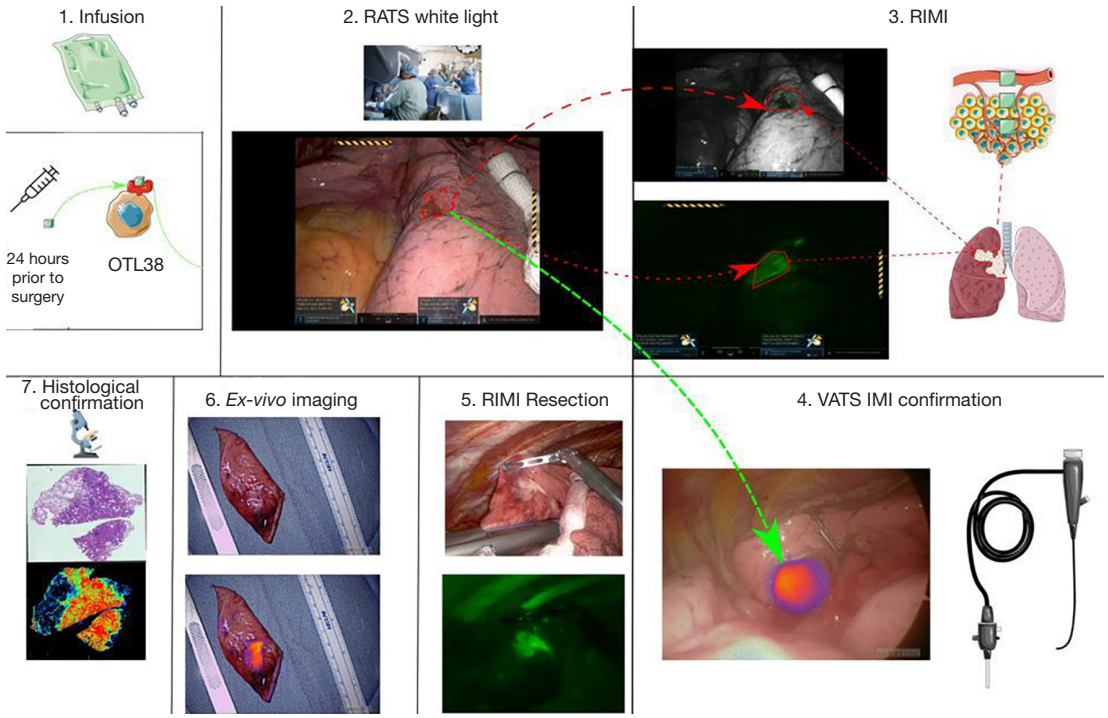

Figure 1 Schematic of study design. On the day prior to surgery, patients were infused with OTL38, a folate receptor-targeted near-infrared contrast agent that has been used in previous trials of intraoperative molecular imaging during video-assisted thoracic surgery (VATS-IMI) given known overexpression of folate receptor alpha in pulmonary cancers. On the day of surgery, localization of the lesion was attempted sequentially using white-light thoracoscopy, then IMI during robotic-assisted thoracic surgery (RIMI), and then confirmed with VATS-IMI as a control group. Fluorescence was evaluated on the back table following resection and then confirmed on a microscopic level postoperatively. RATS, robotic-assisted thoracic surgery.

All subjects were scheduled for minimally invasive, robotic-assisted thoracic surgery. On the day prior to resection, study participants received 0.025 mg/kg of OTL38 by intravenous infusion. The 24-hour time between infusion and imaging has been determined previously to yield the highest signal-to-background ratios by minimizing background, off-target fluorescence. During resection, a standard four port RATS technique was utilized. The robotic ports were inserted and a white-light robotic scope was utilized to identify known tumors. RIMI was then conducted. If the preoperatively identified nodule was unidentifiable by white-light thoracoscopy, localization using fluorescence guidance was attempted. Finally, a VATS thoracoscope designed to detect OTL38 (VisionSense, New York, NY, USA) was inserted in the assistant port to assess for lesion fluorescence. This thoracoscope has been extensively validated by our group in previous trials (23,24), and was thus used as a control to compare to RIMI. The lesions were then resected under RIMI guidance. Following resection, a near-infrared (NIR) exoscope designed to detect OTL38 (VisionSense, New York, NY, USA) was used to assess for lesion fluorescence on the back table. Specimens were then submitted for histopathologic examination by a pulmonary pathologist.

Study drug

OTL38 ($C_{61}H_{63}N_9Na_4O_{17}S_4$, MW: 1414.42) is a folate analog conjugated to the NIR dye, S0456. OTL38 is characterized by excitation wavelength of 774–776 nm and emission wavelength of 794–796 nm. OTL38 was designed to target the folate receptor which is expressed 90% of pulmonary adenocarcinomas, but has also been shown to target pulmonary squamous cell carcinomas, small cell lung cancer, and granulomas given the expression of folate receptor beta on tumor-associated macrophages (20,26). This drug was provided by OnTarget Laboratories (West Lafayette, IN, USA). The safety and efficacy of OTL38 has

been previously demonstrated in a variety of tumor types (23,24,27,28).

RIMI imaging device

Patients underwent robot-assisted thoracic surgery using the da Vinci Xi system (Intuitive Surgical, Sunnyvale, CA, USA). The da Vinci system consists of three main components: the vision cart, the surgeon console from which the surgeon controls robotic instruments, and the surgical cart from which the robotic arms extend. The Xi model is characterized by three-dimensional vision, which can be enhanced by a fluorescence detection tool, which was customized by Intuitive Surgical to detect OTL38 and termed "Sensitive Firefly". This experimental detection mode provides real-time near-infrared fluorescence imaging with λexcitation at 785 nm and λimaging at 800 nm.

VATS & back table imaging device

In situ, real-time fluorescence imaging was performed during VATS using a 5-mm, 0-degree thoracoscope (VisionSense, New York, NY) optimized for detection of OTL38. This device is a high definition, dual band (white light and NIR) camera system capable of NIR emission and detection. A 785-nm excitation source was utilized, and fluorescence was detected using a bandpass filter ranging from 800 to 835 nm. For *ex vivo* evaluation, a free-standing exoscope with similar optical imaging settings was utilized.

Post-resection specimen analysis

Excised specimens were formalin fixed and paraffin embedded. Sequential 5-µm sections were obtained and underwent comprehensive histopathologic and fluorescence analysis by a board-certified thoracic pathologist. Sections were stained using standard hematoxylin/eosin (H&E) staining. Immunohistochemical (IHC) staining for FRα was performed using a monoclonal antibody, 26B3.F2 (Morphotek Inc., PA, USA) as previously described. Lastly, in order to understand OTL38 accumulation patterns at a microscopic level, an additional unstained 5µm section was evaluated using NIR microscopic scanners (LI-COR, Lincoln, NE & Leica Microsystems Inc, Buffalo Grove, IL, USA).

Post hoc image analysis

Mean fluorescence intensity (MFI) of the lesion (MFI_{lesion}) was obtained by analyzing monochromatic NIR images with ImageJ (http://rsb.info.nih.gov/ij) and measuring the region-of-interest which correlated to the lesion. Background fluorescence (0.5–1.0 cm from margin) was also obtained ($MFI_{background}$). A minimum of 1,000 pixels were included in each measurement. Calculations were repeated in triplicate from varying angles, and signal-to-background fluorescence ratios (SBR) were calculated using the following equation ($MFI_{lesion}/MFI_{background}$). SBR assessments were averaged, and a mean SBR >2.0 was considered fluorescent.

Statistical analysis

All data analysis and statistical comparisons were made using Stata: Release 14 (College Station, TX, USA). A P value less than 0.05 was considered statistically significant.

Results

Patient and lesion characteristics

Between November 2020 and February 2021, ten subjects with pulmonary ground glass opacities underwent RATS resection using IMI guidance from OTL38 infusion. All patients tolerated the full dose of OTL38 infusion and there were no adverse events related to infusion of the study drug. Three subjects were male and seven were female. The median age of subjects at resection was 67.9 years (IQR, 61.25–72.75 years). Preoperative CT and PET were obtained in all subjects and the median lesion size was 1.52 cm (IQR, 1.05–1.93 cm) and most tumors (7/10) were PET-avid with mean SUV of 5.03. Tumors tended to be close to the pleural surface (mean depth 6 mm, IQR, 0–1.0 cm) but pleural puckering was not present on the CT scans of any patient in the study. All patients had clinical stage IA lesions. Four patients had pure GGOs without solid component, and six had GGO with an associated solid component. A full summary of patient and lesion characteristics is provided in *Table 1*.

RATS white light localization of lesions

At the outset of surgery, the standard four arm RATS technique was employed. Before conducting IMI, all lesions were attempted to be localized via white light robotic visualization. Seven of ten (70%) were visually identifiable by pleural puckering, discoloration, or other parenchymal

Table 1 Patient and tumor characteristics

Subject	Age (years)	Sex	Lesion size (cm)	Depth from pleural surface (cm)	GGO type	SUV	Location	Segment	Visualized by white light imaging	Visualized by RIMI	Diagnosis	Wedge resection margin (cm)	Operation performed
1	66	F	1.2	0	Pure GGO	2.9	RLL	Lateral basal	+	+	Invasive adenocarcinoma	0.8	Completion lobectomy
2	84	M	2.2	0.3	GGO with solid component	10.8	RLL	Posterior basal	+	+	Squamous cell carcinoma	0.4	Completion lobectomy
3	78	F	1.2	0.9	Pure GGO	0	RLL	Lateral basal	-	+	Invasive adenocarcinoma	1.0	Completion lobectomy
4	61	F	1.0	0.4	GGO with solid component	0	LLL	Antero-medial basal	+	+	Invasive adenocarcinoma	1.3	Wedge resection
5	56	F	1.7	0.6	GGO with solid component	11.2	RUL	Anterior	+	+	Invasive adenocarcinoma	0.7	Completion lobectomy
6	74	M	1.0	1.3	Pure GGO	0.8	LUL	Superior lingular	–	+	Adenocarcinoma in Situ	1.8	Wedge resection
7	62	F	1.5	0.7	GGO with solid component	3.4	RUL	Apical	+	+	Invasive adenocarcinoma	0.2	Completion lobectomy
8	69	F	2.0	0.4	GGO with solid component	0.1	LUL	Anterior	+	+	Invasive adenocarcinoma	0.2	Completion lobectomy
9	69	M	2.5	0.6	GGO with solid component	1.3	LLL	Superior	+	+	Invasive adenocarcinoma	n/a*	Lobectomy
10	60	F	1.0	1.0	Pure GGO	0.2	LUL	Apico-posterior	–	+	Minimally invasive adenocarcinoma	1.4	Wedge resection

*, this patient did not undergo sublobar resection and proceeded directly to lobectomy. GGO, ground glass opacity; SUV, standardized uptake value; RUL, right upper lobe; RLL, right lower lobe; LLL, left lower lobe; LUL, left upper lobe; RIMI, intraoperative molecular imaging during robotic-assisted thoracic surgery.

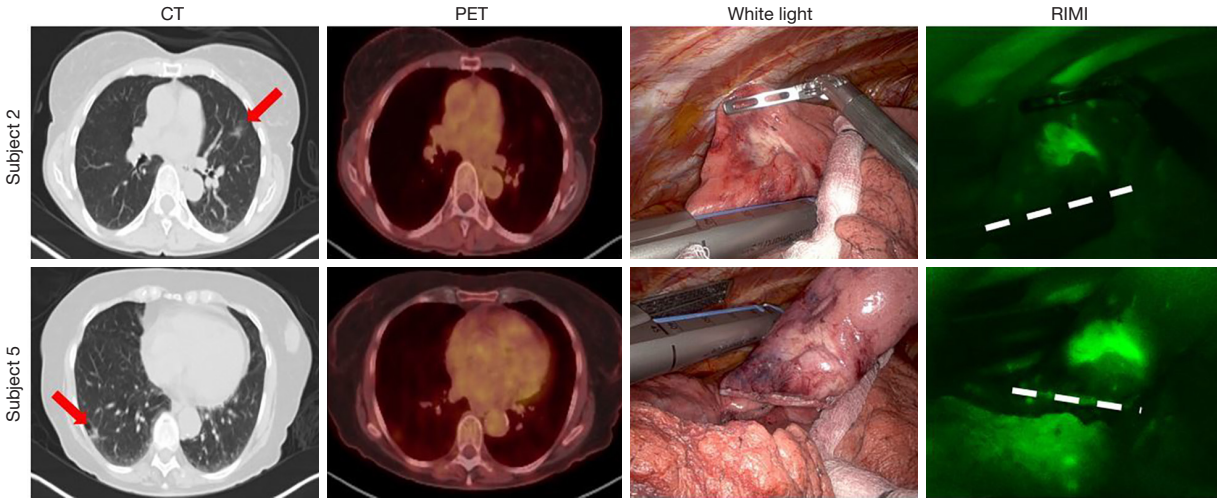

Figure 2 IMI during robotic-assisted thoracic surgery (RIMI) identifies pulmonary GGOs during robotic resection. This figure shows representative images from two patients enrolled in the study. Preoperative CT and PET scans are shown at left, with lesions marked by red arrows. The rightmost two columns show intraoperative white light and near-infrared images, with RIMI clearly identifying both lesions. The dashed line in the rightmost column indicates the stapled resection margin. CT, computed tomography; PET, positron emission tomography; GGOs, ground glass opacities; IMI, intraoperative molecular imaging.

distortion. Those lesions that were not clearly identified were three of the smallest (1.0, 1.0, and 1.2 cm) lesions in the study, all of which were deep to the pleural surface.

RIMI detects tumors during pulmonary resection

Following white light inspection with a standard DaVinci endoscope, *in situ* molecular imaging using the da Vinci "Sensitive Firefly" vision mode was performed. It identified tumor-specific fluorescence signal through the pleural surface in all 10 (100%) subjects. RIMI clearly located the three nodules that could not be seen by robotic white-light imaging. The mean fluorescence intensity (MFI) of tumors was 99.48 arbitrary units (A.U., IQR, 75.72–130.492 A.U.), which was significantly higher than background tissue with mean MFI 20.61 A.U. (IQR, 13.50–29.934 A.U., P<0.0001). Mean signal-to-background ratio was 5.70 (range, 2.28–10.13). There was no statistically significant association of lesion depth with MFI or signal-to-background ratio of the GGO lesions.

VATS-IMI detects tumors during pulmonary resection

For purposes of a control comparison, following RIMI, we imaged all patients with a VATS-IMI thoracoscope though a fifth "assistant" port. This thoracoscope was specifically designed to detect OTL38 and has been extensively validated by our group and others. This served as a control against which we could compare RIMI technology. VATS-IMI was able to detect all (10/10) lesions. Mean fluorescence intensity (MFI) of tumors by VATS-IMI was 117.92 A.U. (IQR, 108.58–133.19 A.U.) and MFI of background parenchyma was 29.30 A.U. (IQR, 22.63–38.53 A.U.). This generated a mean tumor-to-background ratio (TBR) of 5.04 (range, 2.04–11.00). All lesions displayed TBR >2.0, indicating fluorescence.

RIMI allows real-time assessment of margin positivity

Following VATS-IMI, all lesions were resected under guidance from RIMI. Nine of ten (90%) tumors were able to be removed by sublobar pulmonary resection for frozen section pathology analysis. RIMI was used in real time to ensure that the stapled margin was negative for tumor at the initial resection (see *Figure 2* for representative cases), which was confirmed on pathologic analysis. The average resection margin was 0.87 cm (IQR, 0.4–1.3 cm). Six patients subsequently underwent completion lobectomy based upon the intraoperative diagnosis and margin assessment.

Analysis of resected specimens

To further evaluate the fluorescent signal after resection, all specimens were imaged using a NIR exoscope designed to detect OTL38, that has been validated by our group in previous trials (23,24). On back-table analysis, the mean fluorescence intensity (MFI) of tumors was 105.45 A.U. (IQR, 76.94–124.04 A.U.), which was significantly higher than background tissue with mean MFI 18.34 A.U. (IQR, 14.01–18.34 A.U., P<0.0001). Mean signal-to-background ratio was 6.25 (range, 2.45–12.24).

We further performed microscopic analysis of the specimens. On histopathologic analysis, the majority of tumors (n=7, 70%) were invasive adenocarcinomas. There was also a single adenocarcinoma in situ, one minimally invasive adenocarcinoma, and a pulmonary squamous cell carcinoma. Folate receptor staining correlated with tumor location in all patients. The cancers were also located in the area of highest fluorescence intensity on fluorescence microscopy (*Figure 3*).

Comparison of RIMI to VATS-IMI

To evaluate RIMI in the context of existing imaging technology, we compared the imaging characteristics obtained for RIMI to those of VATS-IMI as the gold standard (*Figure 4*). MFI of tumors by VATS-IMI was 117.92 A.U. compared to 99.48 A.U. by RIMI (P=0.13). MFI of background parenchyma by VATS-IMI was 29.29 A.U. compared to 20.61 A.U. by RIMI (P=0.09). There was no significant difference in TBR by imaging modality (mean by RIMI =5.71, VATS-IMI =5.04, P=0.62). In summary, RIMI compared favorably to VATS-IMI by all measured imaging characteristics.

Discussion

Thousands of small, indeterminate pulmonary nodules are detected annually on screening computed tomography scans, a number which is certain to increase in light of recently expanded lung cancer screening guidelines (1,2). These lesions often require resection for diagnosis, but can be difficult to localize intraoperatively, especially in the case of early-stage cancers or *in situ* disease. The challenge of lesion localization is heightened in the case of robotic surgery, which lacks haptic feedback for thoracoscopic palpation (9). This is particularly important for subpleural GGOs, which are just below the pleural lining and have no visual cues such as pleural puckering or retraction. At that juncture, the surgeon is obligated to perform either a large wedge resection or a segmentectomy.

Here, we demonstrate the first-in-human use of IMI for lesion identification during robotic sublobar pulmonary resection. We found that IMI identified all ten tumors with a strong fluorescent signal. Most notable was that RIMI found three lesions that could not be seen with white light imaging. IMI localized tumors with a broad spectrum of pathologies, from invasive adenocarcinomas and squamous cell carcinomas to a small adenocarcinoma in situ. Importantly, IMI facilitated sublobar pulmonary resection in two patients who had small tumors with wide resection margins.

With the rise of minimally invasive thoracic surgery, we anticipate that IMI will continue to gain prominence as an adjunct to the surgeon's ability to localize pulmonary lesions. The increasing use of video-assisted thoracoscopic surgery (VATS) and robot-assisted thoracic surgery (RATS) have been important innovations in reducing operative morbidity for patients and decreasing length of stay. However, these benefits have come at the cost of the removal or distortion of haptic feedback to the surgeon. In robotic surgery, in particular, visual feedback is the primary means by which the surgeon interacts with the surgical field (8,9).

To overcome the lack of tactile feedback in robotic surgery, we anticipate that IMI will have important clinical utility, particularly in the case of small ground glass opacities (GGOs) which often are not easily distinguishable from surrounding lung parenchyma (3). We demonstrate that IMI can help facilitate sublobar resection of these lesions, an important finding as more evidence accumulates showing that sublobar resection is equivalent to formal lobectomy in early-stage pulmonary malignancies within certain populations (4-6).

Furthermore, IMI can help avoid tumor-positive margins while performing robotic pulmonary resection. This real-time feedback in our study helped surgeons particularly with the tumors that were not easily identifiable by visual inspection under white-light cameras. As the technology is refined, we predict that calibrated camera systems will be able to provide quantification of the margin distance from the staple line to the area of the fluorescent lesion, thereby allowing surgeons to rapidly assess the sufficiency of the extent of the resection.

This study adds to the growing body of literature supporting the use of IMI in surgical oncology (17,29,30). Our group and others have demonstrated the efficacy of

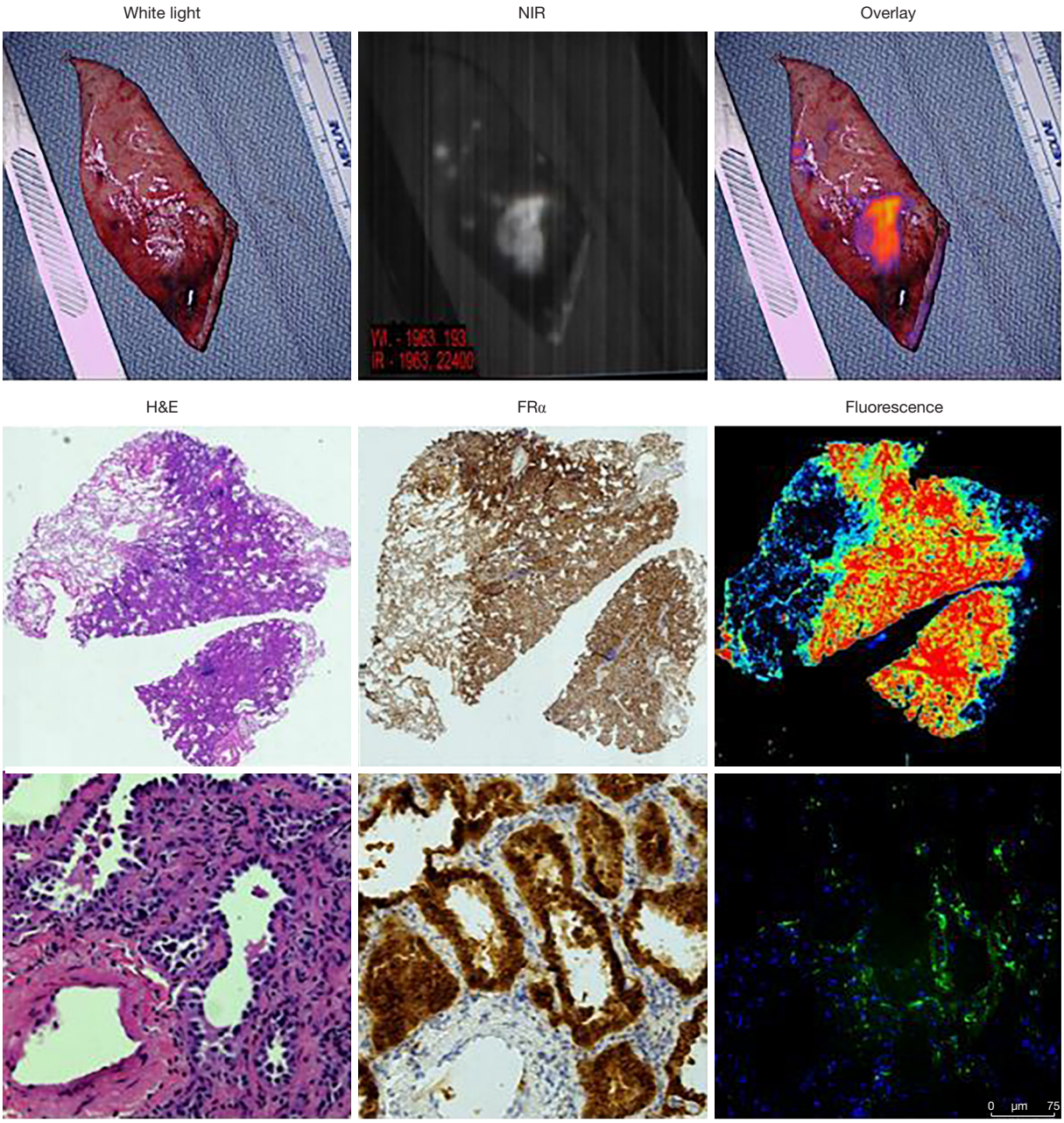

Figure 3 Back table analysis of resected specimens confirms microscopic fluorescence in malignant cells expressing folate receptor alpha. This set of images show representative macroscopic and microscopic fluorescence of a patient enrolled in our study. The middle row shows macroscopic fluorescence images on the back table, showing clear delineation of the tumor by fluorescence. The bottom two rows shows microscopy slides of the tumor tissue stained with hematoxylin-eosin, immunohistochemistry analysis for folate receptor alpha, and correlation with microscopic fluorescence capturing DAPI stain (blue) and OTL38 (green). Top row of photos is original magnification, the middle row is 10× magnification. and the bottom row is 40× magnification. Scale bar shows 75 µm. NIR, near infrared.

IMI in identifying a large range of pulmonary neoplasms during minimally invasive surgery, but the technology has never before been applied to robotic thoracic surgery. This study offers proof-of-concept that IMI is feasible and effective in RATS.

The specific IMI tracer used in this study was OTL38, a

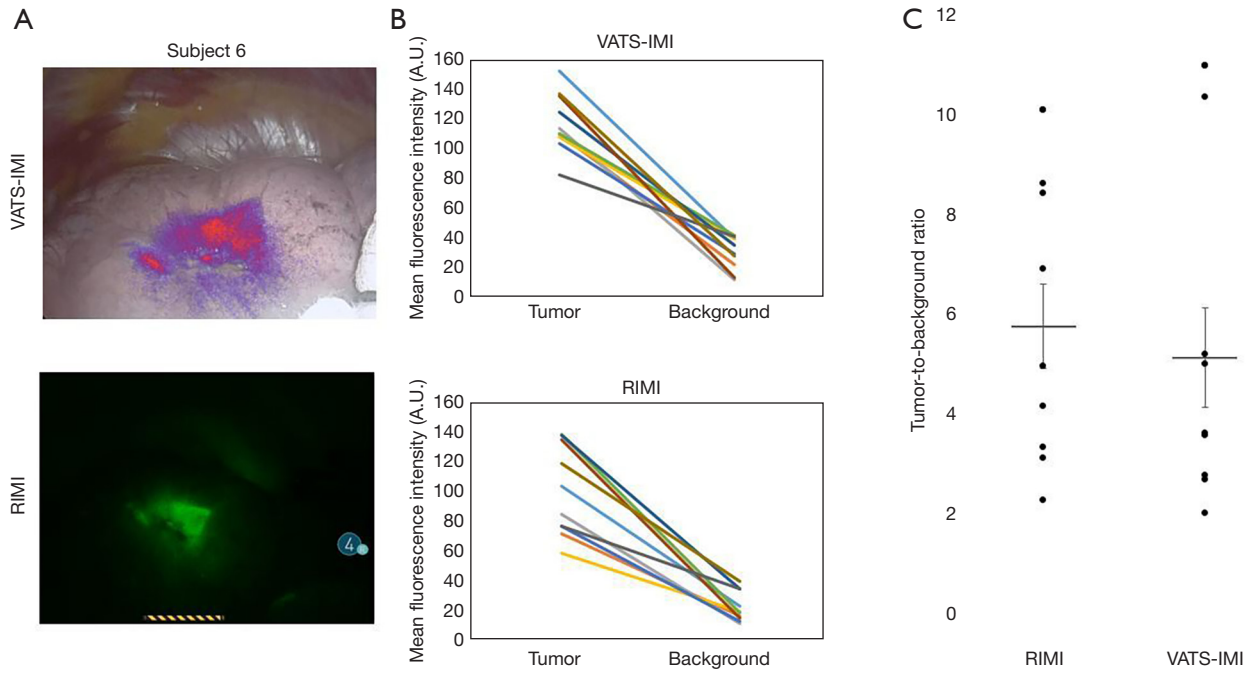

Figure 4 Comparison of IMI during robotic-assisted thoracic surgery (RIMI) to intraoperative molecular imaging during video-assisted thoracic surgery (VATS-IMI). Panel A depicts representative images comparing VATS-IMI and RIMI in the same patient. Panel B shows mean fluorescence intensity (MFI) of lesion and background measurements, stratified by imaging modality (RIMI *vs.* VATS-IMI). Each line links lesion and background measurements from the same subject. Panel C depicts tumor-to-background ratio (TBR) of lesions compared to normal lung parenchyma as background, when stratified by imaging modality. Each point on the plot represents a TBR for an individual patient. Mean TBR was >2 for both RIMI and VATS-IMI, and there were no significant differences between groups. A.U., arbitrary unit; IMI, intraoperative molecular imaging.

folate receptor-targeted fluorophore with signal in the near-infrared spectrum. While the OTL38 tracer was initially designed to target pulmonary adenocarcinomas due to their overexpression of folate receptor-alpha, we have found that the tracer is able to highlight tumors of a broad range of pathologies. These include pulmonary squamous cell carcinomas, small cell lung cancers, and granulomas. We hypothesize in these cases that the tracer is accumulating in the tumor-associated macrophages, which are known to express folate receptor-beta. Further histopathological evaluation in this regard is ongoing by our group.

Despite the heterogeneity of tumors and benign lesions that OTL38 can identify, we do not have definitive data that it can identify every type of GGO lesion. Specifically, we do not know if OTL38 can identify carcinoid tumors or organizing pneumonia that appear radiographically similar to GGO. Therefore, RIMI using OTL38 may not be useful for every etiology of GGO, and further work is needed to understand the specific types of GGOs that OTL38 can identify.

The specific camera used in this study is a modification of the existing DaVinci robotic surgical equipment. IMI is not able to be performed with the standard Firefly imaging technology, which illuminates around 805nm. This study utilized excitation at 785nm and a new fluorescence imaging feature, Sensitive Firefly. Sensitive Firefly is enabled using the daVinci Endoscope Plus and reduces the white light component found in standard Firefly to increase sensitivity to fluorescent media regardless of the excitation wavelength. This specialized camera is an additional cost and current limitation of RIMI, but we anticipate that this cost will be less relevant as wavelength-tunable scopes are developed and standardized for robotic surgery.

We acknowledge several limitations in this study. This was a small trial at a single institution, and needs to be repeated in a larger cohort and at other centers. Furthermore, IMI technology has well-documented limitations in depth of penetration, which was not seen in our study cohort comprised of mostly pleural surface

lesions. Despite these limitations, this trial demonstrates proof-of-principle for the feasibility and efficacy of IMI during robotic sublobar pulmonary resection.

Acknowledgments

Funding: Dr. Kennedy was supported by the American Philosophical Society and the National Institutes of Health (grant F32 CA254210-01). Dr. Azari was supported by the Society for Thoracic Surgeons. Dr. Singhal was supported by the National Institutes of Health (grant R01 CA193556) and the State of Pennsylvania Health Research Formula Fund.

Footnote

Reporting Checklist: The authors have completed the TREND reporting checklist. Available at https://tlcr.amegroups.com/article/view/10.21037/tlcr-21-1004/rc

Data Sharing Statement: Available at https://tlcr.amegroups.com/article/view/10.21037/tlcr-21-1004/dss

Conflicts of Interest: All authors have completed the ICMJE uniform disclosure form (available at https://tlcr.amegroups.com/article/view/10.21037/tlcr-21-1004/coif). GTK reports grant funding from the American Philosophical Society and the National Institutes of Health (grant F32 CA254210-01). SS reports grant funding from the National Institutes of Health (grant R01 CA193556) and the State of Pennsylvania Health Research Formula Fund. NG and JS are paid employees of Intuitive Surgical, Inc. The other authors have no conflicts of interest to declare.

Ethical Statement: The authors are accountable for all aspects of the work in ensuring that questions related to the accuracy or integrity of any part of the work are appropriately investigated and resolved. The study was conducted in accordance with the Declaration of Helsinki (as revised in 2013). The study was approved by the University of Pennsylvania Institutional Review Board (IRB Approval Number: 822153) and all patients gave written informed consent.

References

1. US Preventive Services Task Force; Krist AH, Davidson KW, et al. Screening for Lung Cancer: US Preventive Services Task Force Recommendation Statement. JAMA 2021;325:962-70.
2. Mazzone PJ, Silvestri GA, Patel S, et al. Screening for Lung Cancer: CHEST Guideline and Expert Panel Report. Chest 2018;153:954-85.
3. Pedersen JH, Saghir Z, Wille MM, et al. Ground-Glass Opacity Lung Nodules in the Era of Lung Cancer CT Screening: Radiology, Pathology, and Clinical Management. Oncology (Williston Park) 2016;30:266-74.
4. Wolf AS, Swanson SJ, Yip R, et al. The Impact of Margins on Outcomes After Wedge Resection for Stage I Non-Small Cell Lung Cancer. Ann Thorac Surg 2017;104:1171-8.
5. Altorki NK, Yip R, Hanaoka T, et al. Sublobar resection is equivalent to lobectomy for clinical stage 1A lung cancer in solid nodules. J Thorac Cardiovasc Surg 2014;147:754-62; Discussion 762-4.
6. Dai C, Shen J, Ren Y, et al. Choice of Surgical Procedure for Patients With Non-Small-Cell Lung Cancer ≤ 1 cm or > 1 to 2 cm Among Lobectomy, Segmentectomy, and Wedge Resection: A Population-Based Study. J Clin Oncol 2016;34:3175-82.
7. Aliperti LA, Predina JD, Vachani A, et al. Local and systemic recurrence is the Achilles heel of cancer surgery. Ann Surg Oncol 2011;18:603-7.
8. Okusanya OT, Hess NR, Luketich JD, et al. Infrared intraoperative fluorescence imaging using indocyanine green in thoracic surgery. Eur J Cardiothorac Surg 2018;53:512-8.
9. Hagen ME, Meehan JJ, Inan I, et al. Visual clues act as a substitute for haptic feedback in robotic surgery. Surg Endosc 2008;22:1505-8.
10. Azari F, Kennedy G, Singhal S. Intraoperative Detection and Assessment of Lung Nodules. Surg Oncol Clin N Am 2020;29:525-41.
11. Keating J, Newton A, Venegas O, et al. Near-Infrared Intraoperative Molecular Imaging Can Locate Metastases to the Lung. Ann Thorac Surg 2017;103:390-8.
12. Kennedy GT, Okusanya OT, Keating JJ, et al. The Optical

Biopsy: A Novel Technique for Rapid Intraoperative Diagnosis of Primary Pulmonary Adenocarcinomas. Ann Surg 2015;262:602-9.
13. Newton AD, Kennedy GT, Predina JD, et al. Intraoperative molecular imaging to identify lung adenocarcinomas. J Thorac Dis 2016;8:S697-704.
14. Kennedy GT, Azari FS, Bernstein E, et al. 3D Specimen Mapping Expedites Frozen Section Diagnosis of Nonpalpable Ground Glass Opacities. Ann Thorac Surg 2021. [Epub ahead of print]. pii: S0003-4975(21)01848-8. doi: 10.1016/j.athoracsur.2021.09.069.
15. Predina JD, Newton A, Kennedy G, et al. Near-Infrared Intraoperative Imaging Can Successfully Identify Malignant Pleural Mesothelioma After Neoadjuvant Chemotherapy. Mol Imaging 2017;16:1536012117723785.
16. Kennedy GT, Azari FS, Bernstein E, et al. Targeted Intraoperative Molecular Imaging for Localizing Nonpalpable Tumors and Quantifying Resection Margin Distances. JAMA Surg 2021;156:1043-50.
17. Tipirneni KE, Warram JM, Moore LS, et al. Oncologic Procedures Amenable to Fluorescence-guided Surgery. Ann Surg 2017;266:36-47.
18. Predina JD, Fedor D, Newton AD, et al. Intraoperative Molecular Imaging: The Surgical Oncologist's North Star. Ann Surg 2017;266:e42-4.
19. Low PS, Henne WA, Doorneweerd DD. Discovery and development of folic-acid-based receptor targeting for imaging and therapy of cancer and inflammatory diseases. Acc Chem Res 2008;41:120-9.
20. Parker N, Turk MJ, Westrick E, et al. Folate receptor expression in carcinomas and normal tissues determined by a quantitative radioligand binding assay. Anal Biochem 2005;338:284-93.
21. Tie Y, Zheng H, He Z, et al. Targeting folate receptor β positive tumor-associated macrophages in lung cancer with a folate-modified liposomal complex. Signal Transduct Target Ther 2020;5:6.
22. Puig-Kröger A, Sierra-Filardi E, Domínguez-Soto A, et al. Folate receptor beta is expressed by tumor-associated macrophages and constitutes a marker for M2 anti-inflammatory/regulatory macrophages. Cancer Res 2009;69:9395-403.
23. Predina JD, Newton AD, Keating J, et al. A Phase I Clinical Trial of Targeted Intraoperative Molecular Imaging for Pulmonary Adenocarcinomas. Ann Thorac Surg 2018;105:901-8.
24. Gangadharan S, Sarkaria IN, Rice D, et al. Multi-institutional phase 2 clinical trial of intraoperative molecular imaging of lung cancer. Ann Thorac Surg 2021;112:1150-9.
25. Tummers WS, Warram JM, Tipirneni KE, et al. Regulatory Aspects of Optical Methods and Exogenous Targets for Cancer Detection. Cancer Res 2017;77:2197-206.
26. Predina JD, Newton AD, Xia L, et al. An open label trial of folate receptor-targeted intraoperative molecular imaging to localize pulmonary squamous cell carcinomas. Oncotarget 2018;9:13517-29.
27. Newton AD, Predina JD, Frenzel-Sulyok LG, et al. Intraoperative Molecular Imaging Utilizing a Folate Receptor-Targeted Near-Infrared Probe Can Identify Macroscopic Gastric Adenocarcinomas. Mol Imaging Biol 2021;23:11-7.
28. Randall LM, Wenham RM, Low PS, et al. A phase II, multicenter, open-label trial of OTL38 injection for the intra-operative imaging of folate receptor-alpha positive ovarian cancer. Gynecol Oncol 2019;155:63-8.
29. Hernot S, van Manen L, Debie P, et al. Latest developments in molecular tracers for fluorescence image-guided cancer surgery. Lancet Oncol 2019;20:e354-67.
30. Lauwerends LJ, van Driel PBAA, Baatenburg de Jong RJ, et al. Real-time fluorescence imaging in intraoperative decision making for cancer surgery. Lancet Oncol 2021;22:e186-95.

Cite this article as: Kennedy GT, Azari FS, Bernstein E, Marfatia I, Din A, Deshpande C, Galvis N, Sorger J, Kucharczuk JC, Singhal S. First-in-human results of targeted intraoperative molecular imaging for visualization of ground glass opacities during robotic pulmonary resection. Transl Lung Cancer Res 2022;11(8):1567-1577. doi: 10.21037/tlcr-21-1004

